POLITECNICO DI TORINO
Repository ISTITUZIONALE

Metrological Comparison of Indirect Calibration Methods for Nanoindentation: A Bootstrap-Based Approach

Original
Metrological Comparison of Indirect Calibration Methods for Nanoindentation: A Bootstrap-Based Approach / Maculotti, G., Giorio, L., Genta, G., Galetto, M.. - In: MATERIALS. - ISSN 1996-1944. - 18:18(2025), pp. 1-19. [10.3390/ma18184382]

Availability:
This version is available at: 11583/3006390 since: 2026-01-09T11:10:23Z

Publisher:
Multidisciplinary Digital Publishing Institute (MDPI)

Published
DOI:10.3390/ma18184382

Terms of use:

This article is made available under terms and conditions as specified in the corresponding bibliographic description in the repository

Publisher copyright

(Article begins on next page)

19 November 2026

materials

MDPI

Article

Metrological Comparison of Indirect Calibration Methods for Nanoindentation: A Bootstrap-Based Approach

Giacomo Maculotti [1,*], Lorenzo Giorio [2], Gianfranco Genta [1] and Maurizio Galetto [1]

[1] Department of Management and Production Engineering, Politecnico di Torino, Corso Duca degli Abruzzi 24, 10129 Turin, Italy; gianfranco.genta@polito.it (G.G.), maurizio.galetto@polito.it (M.G.)
[2] Department of Applied Science and Technology, Politecnico di Torino, Corso Duca degli Abruzzi 24, 10129 Turin, Italy; lorenzo.giorio@polito.it
* Correspondence: giacomo.maculotti@polito.it

Abstract

Area shape function and frame compliance are the most critical parameters in nanoindentation, as they control measurement accuracy and represent the largest contributions to measurement uncertainty. Despite the availability of direct calibration methods, indirect calibrations are the most practical and fast. Thus, the indirect calibration methods proposed in ISO 14577-2 are most typically applied in academic and industrial research, as well as in quality controls. Previous research has highlighted some criticalities, but a holistic metrological framework was missing. This work aims to compare the performances of indirect calibration methods for area shape function and frame compliance in the nano-range, considering different alternatives suggested in the standard and most recent literature. The comparison will be based on uncertainty estimation using bootstrap estimation, which will innovatively highlight and introduce the effect of the nanoindentation dataset in the uncertainty estimation. The results show that the optimization of accuracy and uncertainty in mechanical characterization is achieved by indenting pairs of certified reference materials, resulting in a more robust approach to calibration experimental conditions than methods that require a single sample to be indented.

Keywords: nanoindentation; instrumented indentation test; calibration; uncertainty; bootstrap; frame compliance; indenter calibration

check for updates

Academic Editors: Gesheng Xiao, Erqiang Liu and Xiaochao Jin

Received: 30 July 2025
Revised: 8 September 2025
Accepted: 16 September 2025
Published: 19 September 2025

Citation: Maculotti, G.; Giorio, L.; Genta, G.; Galetto, M. Metrological Comparison of Indirect Calibration Methods for Nanoindentation: A Bootstrap-Based Approach. *Materials* **2025**, *18*, 4382. https://doi.org/10.3390/ma18184382

Copyright: © 2025 by the authors. Licensee MDPI, Basel, Switzerland. This article is an open access article distributed under the terms and conditions of the Creative Commons Attribution (CC BY) license (https://creativecommons.org/licenses/by/4.0/).

1. Introduction

The Instrumented Indentation Test (IIT) in the nano-range is a depth-sensing characterization method [1,2]. Although it was originally conceived as a hardness scale capable of overcoming the limits inherent in the optical resolution of conventional hardness scales, it immediately became highly attractive to practitioners [3].

Nanoindentation enables the mechanical characterization of surface layers [4] in terms of hardness, Young's modulus estimation, creep, relaxation [5], and toughness [6], while showing a high resolution that can resolve microstructural phases [7,8] and characterize micro- and nano-components [3]. Recently, nanoindentation has found applications in cutting-edge fields such as energy harvesting devices, i.e., micro nano pillars and nanowire characterization [9]; optoelectronics materials [10]; semiconductors, i.e., for characterizing mechanical properties correlated to energy efficiency and passivation [11]; phase transformation [12]; coatings structure [13,14]; and thickness characterization [15]. More recent and advanced applications leverage nanoindentation's capability of performing

high-temperature characterization to identify material properties and temperature-induced phase changes [16], to characterize residual stress [17,18] and dislocation density [19], to study super elasticity, and shape memory in advanced materials [20] and soft materials, e.g., solgels [21], polymers [22,23], and biomaterials, e.g., hydrogels [24,25], artificial tissues [26,27], natural fibres [28], and for early cancer diagnosis [29,30].

IIT consists of applying a force-controlled indentation cycle of loading, holding, and unloading to a sample by means of an indenter. During the cycle, the applied force (F) and the indenter penetration depth (h) are measured continuously. Figure 1 shows the resulting indentation curve, i.e., $F(h)$.

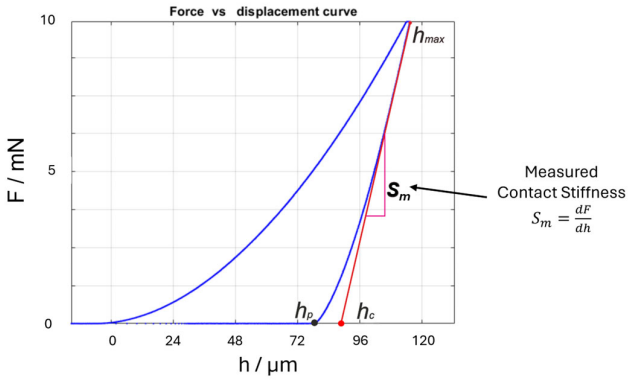


Figure 1. Indentation curve (*IC*): applied force (F) as a function of the penetration depth (h), with highlighted parts showing the corrected depth (h_c), the residual penetration depth (h_p), and the measured contact stiffness (S_m).

Mechanical characterization is achieved, as described by ISO 14577-1 [5], in terms of indentation modulus E_{IT}, i.e., estimating the Young's modulus, and in terms of indentation hardness H_{IT}.

$$E_{IT} = \frac{1-\nu_s^2}{\frac{2\sqrt{A_p(h_{c,max})}}{S\sqrt{\pi}} - \frac{1-\nu_i^2}{E_i}} \tag{1}$$

$$H_{IT} = \frac{F}{A_p(h_{c,max})} \tag{2}$$

$$h_{c,max} = h_{max} - h_0 - C_f F_{max} - \varepsilon \frac{F_{max}}{\frac{1}{S_m} - C_f} \tag{3}$$

$$S_m = \left.\frac{\partial F}{\partial h}\right|_{h_{max}} \tag{4}$$

$$C_{tot} = \frac{1}{S_m} = \frac{1}{S} + C_f \tag{5}$$

where ν_s is the sample's Poisson's ratio, ν_s is the indenter's Poisson's ratio, and E_i is the indenter's Young's modulus. $A_p(h_{c,max})$ is the projected contact area at the maximum corrected penetration depth $h_{c,max}$ and S is the sample contact stiffness. The corrected contact depth is obtained, as per Equation (3), by correcting the measured penetration for the zero contact point error, h_0, and for the elastic displacement of the sample, $\varepsilon \frac{F_{max}}{\frac{1}{S_m} - C_f}$, and of the indentation platform, $C_f F_{max}$. In particular, ε is an indenter geometry-related parameter, S_m is the measured contact stiffness, defined in Equation (4), and C_f is the frame compliance. The sample contact stiffness S is estimated by analyzing the unloading curve, modelling the indentation platform–sample system as a set of springs in series according to Equation (5).

It is worth noticing that the key feature that allows the achievement of nano-scale characterization is the relationship between the contact area and the penetration depth, i.e., the area shape function A_p, typically expressed as a sum of rational monomials as in Equation (6) [2,5].

$$A_p(h) = \sum_{n=0}^{8} a_n h_c^{2-n} \tag{6}$$

The metrological evaluation of nanoindentation has long been investigated to ensure accurate, traceable, and precise material characterization, with the reporting of measurement uncertainty. ISO 14577-2 describes the calibration of the most relevant influence factors [31]. The calibration of force and displacement sensors allows for traceable measurements. However, further influencing factors are most impactful on uncertainty evaluation [32]. On the one hand, the surface integrity is liable for dominating measurement uncertainty by largely increasing the reproducibility [5]. In stable conditions, the most relevant contributors are the area shape function parameters a_n, the frame compliance C_f, the contact stiffness S_m, and the first contact point h_0 [32].

The evaluation of S_m and h_0 significantly impacts both accuracy and precision, depending on the chosen algorithm for their evaluation [32–34]. The literature has shown that among ISO standard methods, the Power Law (PL) method allows for the most accurate and precise material mechanical characterization [32]. In particular, the loading and unloading curves can be modelled as per Equation (7a,b) as follows:

$$h = \alpha_l (h - h_0)^{m_l} \tag{7a}$$

$$h = \alpha_u (h - h_p)^{m_u} \tag{7b}$$

where α and m are material and indenter geometry related parameters, the subscripts l and u stand for loading and unloading, respectively, and α and m, h_0 and h_p are obtained by the non-linear least square fitting of the relevant portion of the indentation curve [5]. Further approaches have been developed, and direct derivative evaluation methods have been proven to provide an estimation of the S_m that is consistent with the ISO 14577-1 approaches, but with a substantially improved uncertainty [35,36].

Conversely, the area shape function parameters and the frame compliance are calibrated; thus, they not only significantly affect the accuracy and uncertainty but also contribute to the traceability of the method. When discussing the calibration of area shape function and frame compliance, it is first relevant to recall that the measurand are, respectively, the geometrical description of the projected area as a function of the penetration depth, i.e., as a function of the indenter height—for pyramidal indenters—or the radius parallel to the loading direction—for spherical indenters—and the compliance to be ascribed to the machine inducing elastic deformation at the measured penetration depth. The area shape function and the frame compliance, as explicated in Equation (3) and in Equation (5), are necessary to account for the fact that the system is not ideal. In fact, both manufacturing errors and wear, generated by mechanical friction and impurity attachment, e.g., by heat, chemical affinity, make the indenter deviate from the nominal geometry, i.e., an ideally sharp pyramid or a perfect sphere. Such deviations introduce severe bias, which, if not corrected, is most severe at the nano and low micro scale. The frame compliance, on the other hand, accounts for the fact that the system is not infinitely stiff. Thus, the system, due to reaction forces, is subjected to elastic deformations that add up to the measured penetration depth, becoming most significant for higher loads.

1.1. Calibration Methods for Area Shape Function and Frame Compliance

The literature describes several calibration methods for area shape function parameters a_n and the frame compliance C_f. These calibration methods can be distinguished into direct and indirect approaches.

Direct calibration methods require directly estimating the measurand by a measuring instrument that is traceable. For the area shape function, this is typically achieved using surface topography measuring instruments, which are most suitable for calibrating indenters used for micro- and macro-scale IIT. Several examples can be found in the literature. Typically, national metrological institutes rely on confocal microscopes or coherence scanning interferometers [37], and measurement uncertainty propagation may require the non-trivial linear algebra modelling of geometrical entities [38]. Conversely, at the nano-scale, atomic force microscopy (AFM) is required [39–41]. Such an alternative is particularly challenging for extended measurements in both the z-height range and x-y range, possibly requiring stitching, and for deformation and cross-talks of scanning axes [41,42]. The direct calibration of frame compliance can be achieved by compensation balances [43] or springs of known stiffness whose the design and material depend on the force scale, e.g., silicon for the nano-scale [44], or more robust alternatives for the macro-scale [45].

Indirect calibration methods are based on statistical analysis using the fundamental equations of nanoindentation of data collected by indenting one or more reference materials at different loads. Indirect calibration methods are most commonly used thanks to their great practicality, speed, and simplicity compared with direct calibration methods. On the other hand, the uncertainty of calibrated parameters results in larger contributions. Several indirect calibration methods have been proposed; some are suitable only for the macro-scale, some for the nano-scale, and others can be applied to both.

ISO 14577-2 considers some calibration methods, which are typically applied in research laboratories and implemented in testing machine software by manufacturers [31]. Table 1 summarizes the methods currently in use according to the standard. As Table 1 shows, ISO 14577-2 only considers indirect calibration methods for C_f, while direct calibration is also suggested for the area shape function. As mentioned, methods requiring direct calibration of the area shape function, i.e., method #1 [46] and #3 [47], are rarely of interest for industrial and academic applied research laboratories, which, thus, mostly resort to method #2 [48] and #4 [49] for Berkovich and Vickers indenters. Indirect calibration methods require collecting sets of at least 10 indentations at different loads on one or two reference materials. These materials must be suitable to enhance measurand effects, that is, a quite stiff material, e.g., tungsten (W), to maximize the contribution of machine elastic deformation to penetration depth for the frame compliance calibration, and a more elastic material, e.g., Al or SiO_2 (fused silica "FS"), to allow large penetration depths at small load to increase the accuracy of the area calibration. Method #5 is specific to spherical indenters, while method #6 has been introduced in the latest draft version of the standard for the micro- and macro-ranges.

Table 1. ISO 14577-2 calibration methods. Notes provide procedural suggestions, including application scope and certified reference materials (CRMs) to be used.

Method #	A_p Calibration	C_f Calibration	Input Required	Notes
1	Direct by AFM	Indirect	A_p calibration	CRM: W
2	Indirect	Indirect	None	CRM: Al, or SiO_2
3	Direct by AFM	Indirect	A_p calibration, calibrated E_r	CRM: W
4	Indirect	Indirect	Calibrated $E_{r,1}$, $E_{r,2}$	CRM 1 (A_p): SiO_2; CRM 2 (C_f): W
5	Indirect	Indirect	Calibrated $E_{r,1}$, $E_{r,2}$, elastic deformation	For spherical indenters
6	Indirect	Indirect	None	For micro- and macro-range (CRM shall not exhibit indentation size effect, nor significant pile-up and sink-in)

Some calibration methods might require the use of a certified reference material (CRM) calibrated in terms of E_r, i.e., the reduced modulus defined as

$$E_r = \left(\frac{1 - \nu_s}{E_{IT}} + \frac{1 - \nu_i}{E_i} \right)^{-1} \quad (8)$$

while others, i.e., method #2 and #6, allow for autocalibration.

Following the previous brief discussion, the next sections discuss the most commonly resorted to standard calibration method for the nano-range. The discussion is limited to the calibration of a Berkovich indenter. First, a brief description of standard methods is provided along with a discussion of some procedural limitations highlighted in the literature, which prompted the development of a further alternative.

1.1.1. ISO 14577-2 Method #2 (M2)

This method is the most commonly applied in research laboratories and implemented in the software of testing machines. It requires collecting $J \geq 10$ indentations at I force levels. Since the calibration method aims to estimate both frame compliance and area shape function parameters, a relatively elastic material should be used, such as SiO_2 or Al. The latter, however, is greatly affected by pile-up and may not be an actual ideal choice.

The method, as defined in ISO 14577-2, is an autocalibration method, as no external reference is required. Once the IJ indentations have been collected, the maximum force F_{max}, maximum penetration depth $h_{max,}$ and measured contact stiffness S_m are evaluated (step 1 of Figure 2), and the problem is initialized assuming an ideal indentation testing machine, i.e., having infinite stiffness ($C_f = 0$), and ideal indenter geometry ($A_p = 24.49 h_{max}^2$), i.e., respectively, step 2 and 3 of Figure 2. Then, a linear regression is performed based on Equation (5) to obtain a first estimate of the frame compliance. Here, it is worth noticing that if the autocalibration approach is applied, i.e., E_r is not known and calibrated, the regression of Step 4 also estimates the ratio $\beta = \frac{\sqrt{\pi}}{2E_r}$ which is then used in the iteration cycle. The first attempt value of C_f allows the estimation of the corrected contact depth (step 5), which is used as a regressor term for the known A_p—estimated (in step 6) by the fundamental relationship between E_r (obtained as β^2), S, and A_p—for estimating regression parameters of the area shape function (in step 6). Then, from the estimation of the projected contact area (in step 7), the process is iterated until convergence is achieved.

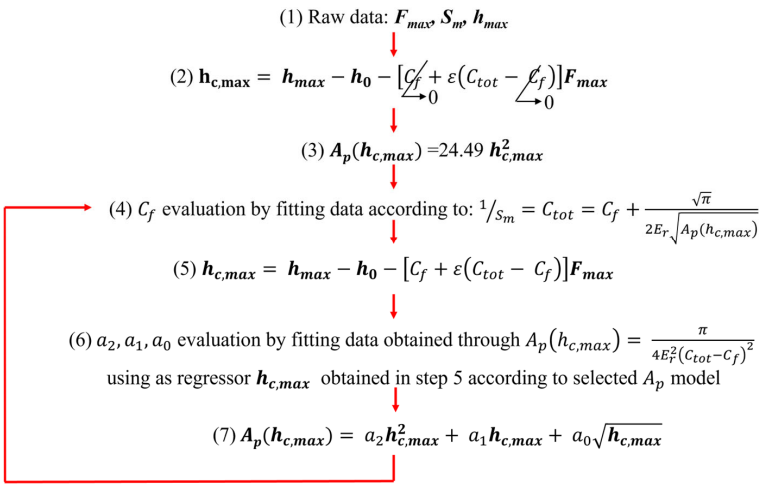


Figure 2. The iterative process for the application of the indirect calibration of area shape function parameters and frame compliance as per ISO 14577-2 methods #2 and #4. The M4 requires carrying out step 4 on the stiffer material (W) and step 6 on the more elastic material (SiO_2). Step 7 shows one of the several possible models for the A_p. Adapted from [50].

1.1.2. ISO 14577-2 Method #4 (M4)

This approach is a variation on M2. It requires performing two sets of $J \geq 10$ indentations at I force levels on two CRMs (see Table 1). The method then proceeds by applying the iterative procedure outlined in Figure 2 and described in the previous Section 1.1.1. The differences lie in the fact that the steps aimed at evaluating the C_f, i.e., steps 3, 4, and 7, are performed on data collected on the stiffer sample, e.g., W; conversely, steps that allow the evaluation of the area shape function parameters, i.e., steps 5, and 6, are performed on data collected on the more elastic sample, e.g., SiO_2. Also, since samples are calibrated CRM, E_r is known, so the regression in step 4 shall not estimate the coefficient of the regressor term $\frac{1}{\sqrt{A_p(h_{c,max})}}$.

1.1.3. Remarks on ISO 14577-2 M2 and M4

The literature highlights the use of known E_r for the samples, i.e., M4 converges much faster than M2 [31,48,49]. Also, from a statistical perspective, the regressions implemented in steps 4 and 6 are constrained linear least squares problems. Specifically, step 4 requires estimating C_f such that it satisfies $C_f > 0$, to reflect the physical meaning of the compliance of a mechanical system. Conversely, the constraint for the slope of the model, i.e., $\beta = \frac{\sqrt{\pi}}{2E_r}$, depends on the applied method. For M2, since it is an autocalibration, it is only required that $\beta > 0$. On the other hand, for M4, since calibrated CRMs are used, the actual regressor term can be considered $\frac{\beta}{\sqrt{A_p(h_{c,max})}}$. This implies that the slope of the estimated model has to be equal to 1. This constraint for practical implementation, due to numerical solution, can be constrained to $[1-\eta; 1+\eta]$, where η is a positive, small enough real value, e.g., 0.005. Similarly, constraints are required for the regression of step 6. In particular, $a_2 > 0$, for it is linked to the geometry of the indenter. More stringent requirements can be enforced, e.g., $a_2 = 24.49$ for a modified Berkovich indenter, but the literature has shown that this yields a very large uncertainty on the A_p [51]. Furthermore, it is critical to constrain the linear least squares problem such that $A_p > 0$. This is a computationally non-trivial requirement. In fact, most relevantly for M4, some estimated parameter sets may lead, for very small $h_{c,max}$, to negative areas. This is not only physically impossible in practice but also leads to numerical issues in the iterative procedure when estimating A_p on the stiffer material (in step 7) to move to the next iteration cycle.

Lastly, it is worth noting that if the indenter area shape function is independently and directly calibrated, method #1 and method #3 can be applied. In particular, the procedure of M1 requires applying steps from step 4 onwards of the iterative approach until convergence is achieved, also estimating β with similar constraints as for M2. Conversely, M3 allows a simpler model, as for M4 since it requires a calibrated E_r, as reported in Table 1.

1.1.4. Single-Step Calibration Method (ODR)

From a mathematical perspective, the iterative approach implemented by ISO 14577-2 M2 and M4 ultimately attempts to solve a regression for parameters C_f and a_n. Accordingly, the literature more recently has proposed a more formal rewriting of the approach [50]. The approach requires collecting $J \geq 10$ indentations at I force levels on two CRMs, and solving the multivariate non-linear regression as follows:

$$\begin{cases} \frac{\pi}{4E_r^2} = \left(\frac{1}{S_m} - C_f\right)^2 \left\{a_2\left[h_{max} - h_0 - \left[C_f + \varepsilon\left(\frac{1}{S_m} - C_f\right)\right]F_{max}\right]^2 + a_1\left[h_{max} - h_0 - \left[C_f + \varepsilon\left(\frac{1}{S_m} - C_f\right)\right]F_{max}\right] + a_0\left[h_{max} - h_0 - \left[C_f + \varepsilon\left(\frac{1}{S_m} - C_f\right)\right]F_{max}\right]^{1/2}\right\} \\ H_{IT} = \frac{F_{max}}{a_2\left[h_m - h_0 - \left[C_f + \varepsilon\left(\frac{1}{S_m} - C_f\right)\right]F_{max}\right]^2 + a_1\left[h_m - h_0 - \left[C_f + \varepsilon\left(\frac{1}{S_m} - C_f\right)\right]F_{max}\right] + a_0\left[h_{max} - h_0 - \left[C_f + \varepsilon\left(\frac{1}{S_m} - C_f\right)\right]F_{max}\right]^{1/2}} \end{cases} \quad (9)$$

The solution to the non-linear regression problem is best addressed by orthogonal distance regression (ODR). ODR accounts for errors in regression variables due to uncertainty in measuring the penetration depth and applied force, as well as in estimating the

first contact point and measured contact stiffness. Since the estimation of the parameters is achieved by solving the regression, this approach can be referred to as a single-step method, as opposed to the standard iterative approach.

The model of Equation (9) is written considering a particular choice of the area shape function; however, other choices are equally applicable, as discussed in Section 1. In particular, Equation (9) is written for a Berkovich indenter assuming a specific truncation of the area shape function reported in Equation (6). By changing the area shape function, it is possible to cater for other approximation models, or for other indenter geometries, e.g., Vickers. Applications of the ODR single-step method to indenter geometries different from Berkovich indenters and to scales larger than nanoindentation are still unreported.

Most relevantly, the ODR single-step method requires the calibration of CRMs in terms of E_r and H_{IT}. The former is conventionally available. The second is more challenging and less trivial, since the indentation hardness is a parameter highly sensitive to both indentation size effect and pile-up and sink-in. However, under the assumption of the ISO 14577-2, the most commonly used CRMs, i.e., SiO_2 and W, are purposely chosen to minimize such effects in indirect calibration methods. From a practical perspective, the calibration of H_{IT} can be obtained using a nanoindentation machine whose C_f and A_p parameters were directly and independently calibrated.

The regression is still subject to constraints, requiring $C_f > 0$ and $a_2 > 0$. With a suitable large range of penetration depths, conveniently achieved by the selection of CRMs, the constraint on $A_p > 0$ is no longer necessary, because it was induced by the iterative process attempting to achieve an independent solution of a coupled problem. Lastly, it is worth highlighting that the ODR solves a total least squares problem weighted for the uncertainty of both regressor and dependent variables, i.e., E_r and H_{IT} [50,52].

1.2. Criticalities of Indirect Calibration Methods

From the previously presented literature review, it is clear that iterative approaches lack a formal statistical definition, which is overcome by the ODR single-step approach [50]. An additional discussion can be prompted by the suggestion provided by the ISO 14577-2, which suggests, for M4, to perform measurements on the stiffer material at much higher forces, i.e., considering a (1–100) mN range for the elastic material and a (100–200) mN range for the stiffer material. This suggestion, although sensitive from a practical perspective, as it allows larger indentations to be performed, introduces a decoupling in the evaluation range of frame compliance and area shape function parameters. The literature has more recently shown that frame compliance is non-linear; thus, such decoupling might be liable to bias the estimation of calibrated parameters. However, investigations of such decoupled force ranges on parameters' calibration are not available, to the authors' best knowledge. Moreover, the ISO 14577-2 states that M4 allows for estimating a non-constant frame compliance. However, since the C_f is estimated as the intercept of a linear model, which is evaluated on a certain force range, the method implies that a constant C_f is actually estimated on the considered force range. A strong piecewise linear approximation of the non-linear behaviour of C_f could be obtained by applying the M4 method on several force ranges.

Furthermore, from an uncertainty evaluation perspective, iterative approaches hinder the application of closed-form estimations, as the law of propagation of uncertainty, because each iteration relies on statistically estimated parameters that have their own variability [50,51,53]. This requires the application of simulative approaches for uncertainty evaluation. The literature has attempted comparisons based on the Monte Carlo method, for which it has been proven more recently that a proper set up is highly critical due to the correlation of input quantities, i.e., the applied force and the penetration depth [54]. Previ-

ous results, based on the Monte Carlo method, showed a substantial impact of the range of *I* maximum forces on the calibrated parameters for the ISO 14577-2 methods [50,51,53]. Moreover, M2 being presented as an autocalibration approach, despite being highly convenient and cheaper, might result in increased measurement uncertainty. More recently, an improved bootstrap-based approach for uncertainty evaluation was proposed. This is particularly convenient for practitioners, for it does not require a strong distributional hypothesis to be performed on input quantities. Conversely, it highlighted a potential severe underestimation of the measurement uncertainty of calibrated parameters when indirect calibrations are performed only on a single set of *IJ* indentations [54]. However, the previously highlighted sensitivity for the number and range of *I* loads was no longer investigated with the most appropriate bootstrap-based uncertainty evaluation. Similarly, no report of such effects is available for the ODR single-step method.

1.3. Scope of the Work

This work focuses on indirect calibration methods for area shape function and frame compliance for nanoindentation. With reference to the criticalities highlighted in Section 1.2, this paper aims to describe the performances of the most commonly used methods suggested in the ISO 14577-2 and of the main alternatives that have been proposed within a metrological framework. This is achieved by comparing the parameters calibrated using diverse methods and assessing their effect on mechanical characterization results, while considering calibration uncertainty. Furthermore, leveraging previous partial investigations in the literature, a structured sensitivity analysis on the main factors liable for affecting the calibration results of such methods, dependent on particular user's choices, will be investigated. Ultimately, this paper aims to provide practical guidelines for the optimal use and implementation of standard calibration methods, while highlighting the potential of other approaches, with the goal of enabling practitioners to minimize the bias and uncertainty of characterization by nanoindentation.

The rest of the paper is structured as follows. Section 2 describes the experiments implemented for the application of selected calibration methods and the approach for the uncertainty evaluation of the results. Section 3 presents the results that are discussed in Section 4. Finally, Section 5 will conclude on the findings.

2. Materials and Methods

This paper aims to compare the sensitivity of the ISO 14577-2 M2 and M4 and of ODR calibration methods to the force range considered for calibration. Furthermore, the effect on the accuracy and precision of autocalibration will be assessed. The comparison will be based on experiments described in Section 2.1 and will assess the effect of different calibration methods on the average and measurement uncertainty of calibrated parameters, namely the frame compliance C_f and the area shape function parameters a_n, as well as on mechanical characterization in terms of the indentation modulus E_{IT}. The comparison will exploit hypothesis tests based on the t-Student distribution and the uncertainty evaluation method described in Section 2.2.

2.1. Experiment Set Up

Indentations were performed by a state-of-the-art Anton Paar (Neuchatel, CH) NHT^3 indentation platform hosted in the metrological room of the Mind4Lab@DIGEP. The indentation instrument was equipped with a Berkovich indenter. The indentation platform features calibrated force transducers with an accuracy of $\pm$1% of the reading and a resolution of 1 nN, and a capacitive displacement sensor with an accuracy of $\pm$0.05% of the reading and a resolution of 0.04 nm. Indentations are performed on a CRM calibrated

by NPL in terms of Young's modulus and Poisson's ratio by the pulse–echo method. Table 2 summarizes the considered maximum loads and the calibrated values for each CRM. For each load, J = 15 replications were performed; each indentation consisted of a force-controlled cycle with a loading to the maximum force and a complete unloading both for 30 s, and a holding time of 10 s (for the SiO_2) and of 60 s (for the W). Measurements are performed with an acquisition frequency of 10 Hz. As can be appreciated from Table 2, a slight decoupling in terms of the investigated force ranges is necessary to avoid the indentation size effect and pile-up to bias measurement results on W. The collected data were used to calibrate the frame compliance and the area shape function of the indenter according to the calibration methods listed in Table 3.

Table 2. CRM properties and tested maximum forces. Intervals of calibrated CRM properties are confidence intervals at a 95% confidence level (k = 2). H_{IT} was evaluated on historical data.

Certified Reference Material	Calibrated Property	Tested Maximum Forces/mN
SiO_2 (FS)	E = (73.0 ± 0.5) GPa υ = (0.163 ± 0.002) H_{IT} = (8.5 ± 0.5) GPa	0.5, 1, 2.5, 5, 7.5, 10, 15, 20
W	E = (414.3 ± 5.6) GPa υ = (0.279 ± 0.005) H_{IT} = (7.0 ± 0.5) GPa	1, 2.5, 5, 7.5, 10, 15, 20

Table 3. Selected calibration methods. I is the number of considered force levels.

Short Name	Applied Method	CRM	Used Force Range/mN	I
M2-FS5	ISO 14577-2 M2 with use of calibrated E_r	SiO_2	[1–10]	5
M2-FS8			[0.5–20]	8
M2AUTOCAL-FS5	ISO 14577-2 M2		[1–10]	5
M2AUTOCAL-FS8			[0.5–20]	8
M4-FS5-W5	ISO 14577-2 M4	SiO_2, W	SiO_2: [1–10] W: [5–20]	5
M4-FS8-W5			SiO_2: [0.5–20] W: [5–20]	A_p: 8 C_f: 5
M4-FS8-W7			SiO_2: [0.5–20] W: [1–20]	A_p: 8 C_f: 7
ODR-FS5-W5	ODR Single-step method	SiO_2, W	SiO_2: [1–10] W: [5–20]	5
ODR-FS8-W5			SiO_2: [0.5–20] W: [5–20]	A_p: 8 C_f: 5
ODR-FS8-W7			SiO_2: [0.5–20] W: [1–20]	A_p: 8 C_f: 7

2.2. Uncertainty Evaluation

The uncertainty of the calibrated parameters is evaluated using a bootstrap approach proposed elsewhere and summarized here. As briefly discussed in Section 1.2, bootstrapping does not require modelling the correlation between the input quantities, i.e., the force and the penetration depth. This greatly simplifies the approach compared with parametric simulative approaches, such as Monte Carlo, which, if applied in a way that neglects the correlation results in an excessive overestimation of measurement uncertainty [54].

The bootstrapping requires for each set of J replicated indentations (at a given i-th load) to resample the experimental curve, which contains B points. The resampling is performed by randomly extracting time-subsequent pairs of $\{F, h\}$ from the J curves. Resampling $\{F, h\}$ pairs allow us to inherently cater for the correlation $F(h)$. Each calibration requires a set of IJ curves. By applying the resampling to each of the I indentation sets collected at different loads, it is possible to simulate a new calibration dataset, i.e., a bootstrap sample.

The number of simulated calibration datasets is $K(< K^{B-1})$. Accordingly, it is possible to perform K calibrations of C_f and a_n. In this work, K = 11,000 simulated calibration datasets were generated.

If we let $\hat{x}$ be any of the calibrated parameters, it is possible to compute the grand average representing the calibrated value as follows:

$$x_{cal} = \bar{\hat{x}} = \frac{\sum_{w=1}^{K} \hat{x}_w}{K}, \tag{10}$$

and—with ANOVA modelling—considering the variability due to the different calibration datasets (variance between s_B^2) and the variability due to the regression (variance within s_W^2) it is possible to firstly assess the significance of the calibration dataset on the calibrated parameter, and secondly to obtain the total variance of the calibrated parameter s_{TOT}^2, by composing the variance between and the variance within, as per Equation (13). In particular, the variance within is obtained as the average of the variance of the regression estimated variability, i.e., the square of the standard error. The last standard error from the iterative procedures can be used for computations. From the total variance, it is possible to estimate the expanded uncertainty of the calibrated parameter, as in Equation (14), which approximates the coverage factor with the value 2, considering the *KIJ-1* degrees of freedom.

$$s_B^2 = IJ \cdot \frac{\sum_{w=1}^{K} (\hat{x}_w - x_{cal})^2}{K-1} \tag{11}$$

$$s_W^2 = \frac{\sum_{w=1}^{K} SE_w^2(\hat{x})}{K} \tag{12}$$

$$s_{TOT}^2 = u^2(\hat{x}) = \frac{s_B^2 \cdot (K-1) + s_W^2 \cdot K(IJ-1)}{KIJ-1} \tag{13}$$

$$U(\hat{x}) = 2s_{TOT} \tag{14}$$

Furthermore, the effect of the possible differences on calibrated parameters on mechanical characterization is assessed. This is investigated for the main mechanical characteristics, i.e., E_{IT}. Additionally, the expanded uncertainty of E_{IT}, i.e., $U(E_{IT}) = 2u(E_{IT})$, is evaluated by applying the law of propagation of uncertainty to their definition reported in Equation (1) [32,54,55], assuming a coverage factor k = 2, corresponding to a confidence level of 95%. The average value of E_{IT} is directly evaluated from experimental data by applying Equation (1) and considering the average of the results.

2.3. Statistical Evaluation of Results

The relevance of the calibration dataset and the effect of different calibration methods will be discussed in terms of the following:

- The distribution shape of the calibrated value $\hat{x}_w$.
- The statistical relevance of the effect of calibration datasets by performing a hypothesis test based on the F-Fisher distribution, with the null hypothesis $H_0 : \frac{s_B^2}{s_W^2} \sim F_{K-1,K(IJ-1)}$, where the degrees of freedom of the numerator are $K-1$ and of the denominator are $K(IJ-1)$.
- The statistical difference in calibrated values by performing a hypothesis test based on the t-Student distribution, with the null hypothesis $H_0 : \frac{\hat{x}_{C1} - \hat{x}_{C2}}{\sqrt{u^2(\hat{x}_{C1}) + u^2(\hat{x}_{C2})}} \sim t_{v_{pooled}}$, where $\hat{x}_{C1}$ and $\hat{x}_{C2}$ are the calibrated parameters from any two methods from Table 3,

and v_{pooled} are the pooled degrees of freedom of the difference $\hat{x}_{C1} - \hat{x}_{C2}$ obtained by the Welch–Satterthwaite formula [55].

- The statistical difference in mechanical characterization results by performing a hypothesis test based on the t-Student distribution, with the null hypothesis $H_0 : \frac{E_{ITC1} - E_{ITC2}}{\sqrt{u^2(E_{ITC1}) + u^2(E_{ITC2})}} \sim t_{v_{pooled}}$.
- Relative accuracy: $\frac{E_{ITCi} - E_{ITref}}{E_{ITref}}$, where E_{ITCi} represents the mechanical characterization from any of the considered calibration methods (in this case, i ranges from 1 to 10), and the E_{ITref} is the reference value reported on the calibration certificate by an independent characterization method.
- Relative uncertainty: $\frac{U(E_{ITCi})}{E_{ITref}}$.

3. Results

The ten different calibration methods were applied according to the experimental plan outlined in Section 2.1. The bootstrap approach was applied to elicit the uncertainty evaluation of the calibrated parameters, and 10,000 bootstrap samples were generated. Figure 3 shows the histogram of the calibrated parameters (C_f) and the area shape function parameters (a_n).

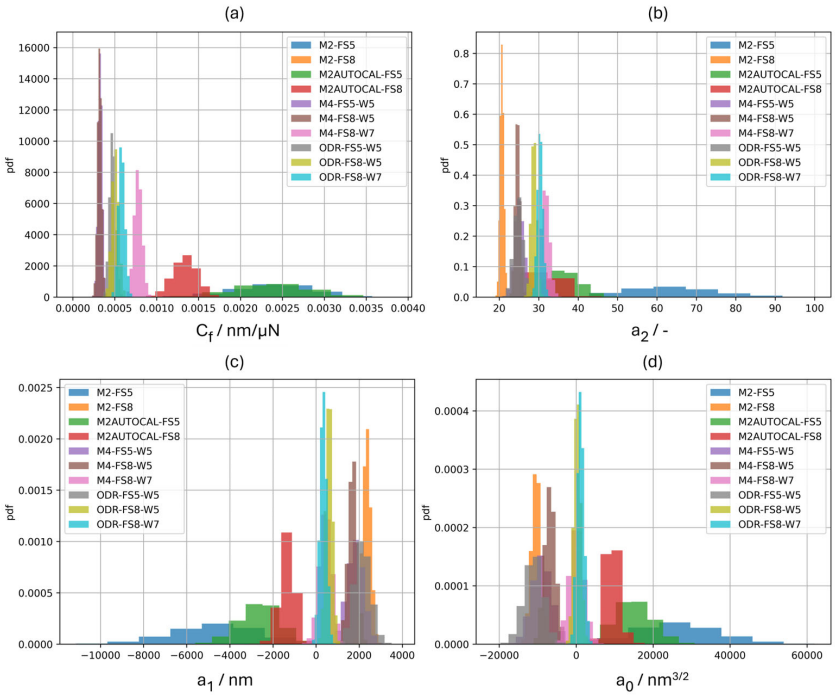


Figure 3. Empirical probability density function (pdf) of the 10,000 calibrated parameters for the 10 calibration methods. (**a**) Frame compliance (C_f): notice the calibration method dependency of the dispersion, and the difference in the average estimates due to different calibration methods. (**b**) a_2: theoretical value is 24.49; notice the significant dependence of both average and dispersion on the calibration method for all area shape function parameters, i.e., also for (**c**) a_1 and (**d**) a_0. Due to the scale, the histogram of C_f for the calibration method M2-FS8 is not reported. Appendix A reports individual histograms for C_f (see Figure A1).

According to Equations (11) and (12), the variance of the mean calibrated parameters (variance between bootstrap sample calibration) and the variance due to regression (variance within bootstrap sample calibration) were estimated and combined to evaluate the total variance of the calibrated parameters.

Table 4 reports, for each calibration method and for each calibrated parameter, whether the contribution to the total variance of the calibrated parameter due to the calibration

dataset (here simulated by bootstrapping), i.e., the variance between, is statistically significant with a risk of error of 5%. Also, the table reports the relative contribution of the bootstrapping to the sum of squares (*SS*), i.e., the product of the variance and the relevant degrees of freedom.

Table 4. *p*-values and relative contribution to sum of squares (SS) due to the indentation dataset variability, which in this work has been obtained by bootstrapping. A relevant contribution is highlighted for *p*-values smaller than 5% (0.05). Notice that the area shape function parameters are most sensitive to the indentation dataset.

	C_f		a_0		a_1		a_2	
Method	***p*-Value**	SS_B/SS_{TOT}	***p*-Value**	SS_B/SS_{TOT}	***p*-Value**	SS_B/SS_{TOT}	***p*-Value**	SS_B/SS_{TOT}
M2-FS5	<0.001	95.7%	<0.001	80.2%	<0.001	87.6%	<0.001	97.0%
M2-FS8	>0.99	<1‰		25.8%		32.8%		43.1%
M2AUTOCAL-FS5	<0.001	95.3%		73.2%		83.0%		93.1%
M2AUTOCAL-FS8	<0.001	68.2%		36.8%		58.6%		95.8%
M4-FS5-W5	>0.99	1.9%		39.5%		43.2%		50.7%
M4-FS8-W5	>0.99	1.8%		27.7%		35.8%		53.7%
M4-FS8-W7	<0.001	6.8%		33.8%		44.4%		70.5%
ODR-FS5-W5	<0.001	38.0%		21.3%		21.0%		19.9%
ODR-FS8-W5	<0.001	47.7%		22.9%		25.6%		36.2%
ODR-FS8-W7	<0.001	40.1%		19.4%		21.6%		30.6%

Confidence intervals with a confidence level of 95%, i.e., with a coverage factor of 2, are reported for the calibrated parameters in Figure 4. Confidence intervals are evaluated from the expanded uncertainty as per Equation (14), and the error bar plots allow for a comparison of the effect of the calibration method.

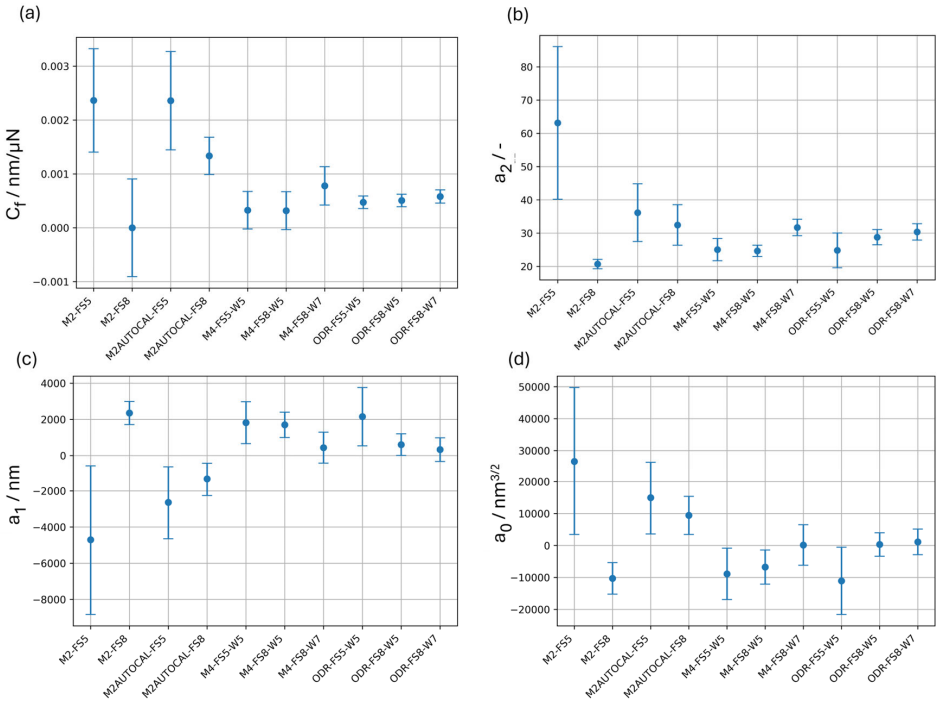


Figure 4. Error bar plots of the calibrated parameters as a function of the calibration method. (**a**) frame compliance, (**b**) a_2, (**c**) a_1, and (**d**) a_0. Error bars represent the expanded uncertainty with a coverage factor of 2 (confidence level of 95%).

Finally, the mechanical characterization of the calibrated samples (see Table 2) has been evaluated in terms of E_{IT}. Figures 5 and 6, respectively, show the validation of the

calibration methods on the SiO_2 and the W CRM, where error bars represent the expanded uncertainty evaluated according to the law of propagation of uncertainty with a coverage factor of 2. Since average values are computed from experimental data, changing only the calibrated values of the area shape function parameters and the frame compliance, any change in the average and the expanded uncertainty in the panels of Figures 5 and 6 must be ascribed to the calibration methods.

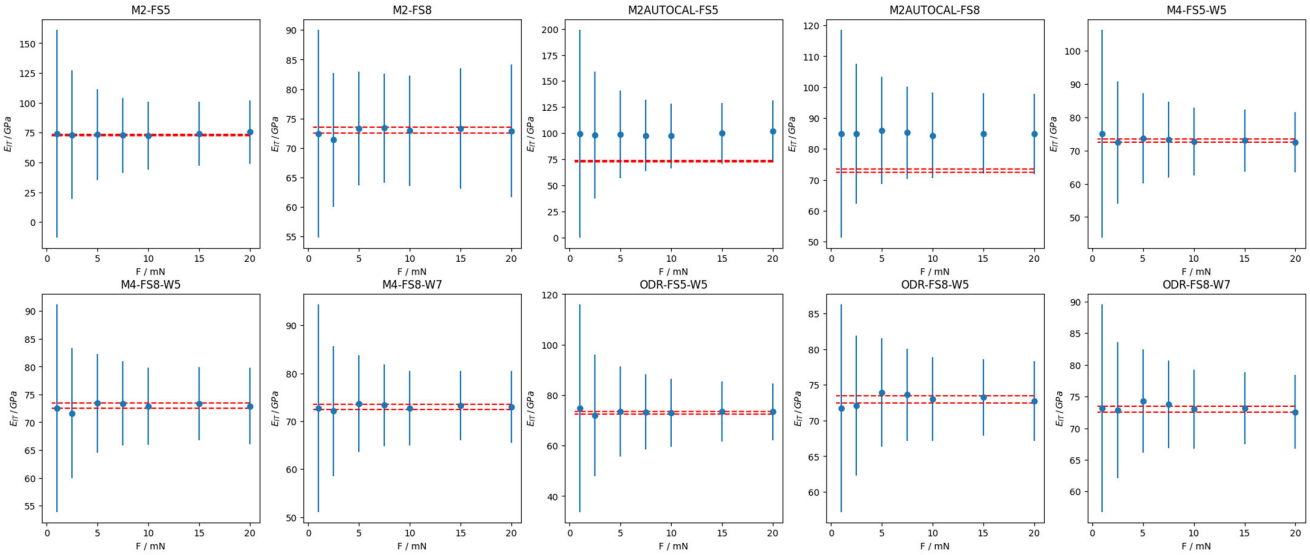


Figure 5. SiO_2 E_{IT} for the different calibration methods. E_{IT} as a function of maximum characterization force. Error bars represent expanded uncertainty (coverage factor of 2). Red dashed lines are the confidence interval for the independently calibrated value of the Young's modulus of the sample.

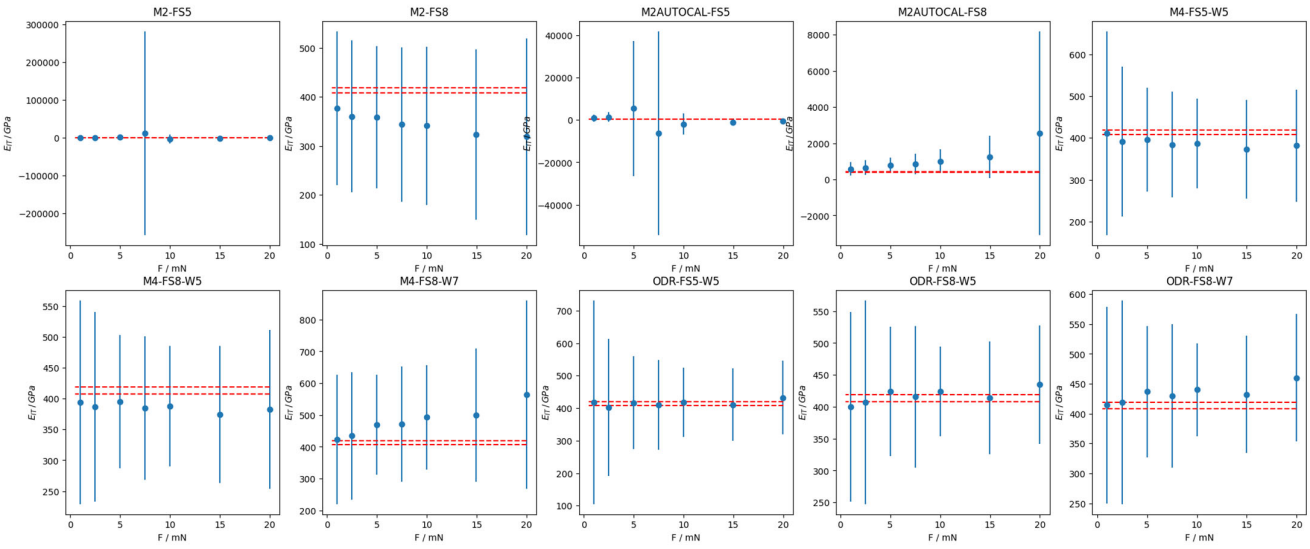


Figure 6. W E_{IT} for the different calibration methods. E_{IT} as a function of maximum characterization force. Error bars represent expanded uncertainty (coverage factor of 2). Red dashed lines are the confidence interval for the independently calibrated value of the Young's modulus of the sample.

The relative accuracy and relative expanded uncertainty for the obtained E_{IT} of the two CRMs are reported in Figure 7a,b, respectively.

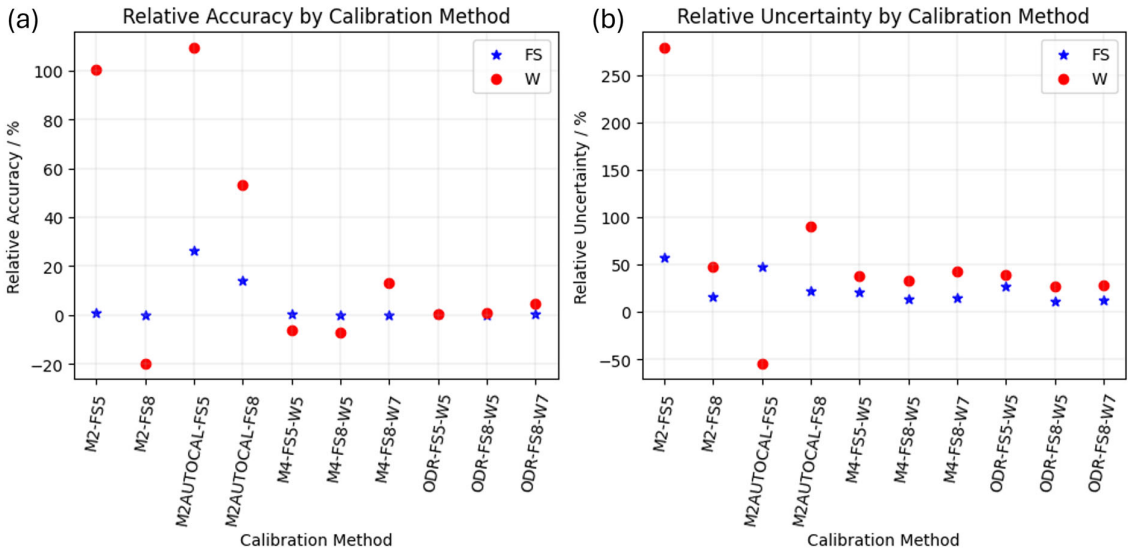


Figure 7. (**a**) Relative accuracy and (**b**) relative uncertainty for the E_{IT} of SiO_2 (FS blue star) and W (red circle). Improved visualization with large values excluded is available in Figure A2.

4. Discussion

As can be seen from Figure 3, the different calibration methods impact the average and the dispersion of the calibrated parameters. In particular, methods based on only one CRM, i.e., M2 and M2AUTOCAL, provide a much larger dispersion of and average C_f and a_2.

The ANOVA, as highlighted in Table 4, shows that for all parameters, the use of a single indentation set (i.e., a group of J replications performed at I loads) is liable to severely underestimating the measurement uncertainty of the calibration parameters. The only exception is represented by the method M4 of ISO 14577-2, when the highest loads are considered for W, i.e., M4-FS5-W5 and M4-FS8-W5. The ANOVA result highlights the need for multiple calibration datasets to be collected to allow a representative estimation of the measurement uncertainty. This can be effectively achieved by bootstrapping to relieve the experimental cost.

Once the total variance is estimated and the expanded uncertainty of the calibrated parameters is evaluated, it is possible to perform hypothesis tests to quantify if the differences are statistically significant. This can be obtained graphically by the error bars in Figure 4. As can be appreciated, methods based on a single CRM, i.e., M2 and M2AUTOCAL, provide a systematically different estimation of all calibrated parameters.

Such results reflect on the evaluation of the mechanical characterization in terms of indentation modulus E_{IT}. On the one hand, as can be appreciated in Figures 5 and 7a, the evaluation of SiO_2, i.e., fused silica (FS), is on average accurate, apart for the exception of the M2AUTOCAL method, which results in a severe, statistically significant bias of more than 15%. On the other hand, as shown in Figures 6 and 7a, methods based on a single CMR have very limited applicability to different materials, yielding severe bias (larger than 50%) and considerably large relative uncertainties.

A closer insight into the methods based on one CRM reveals that autocalibration results in a larger relative uncertainty and poorer accuracy, as highlighted by the comparison of results from M2 and M2AUTOCAL in Figure 7. Furthermore, it is immediately apparent that such methods are sensitive to the range of considered forces. Specifically, the adoption of a larger force range (FS8, which adds larger forces, i.e., 15 mN and 20 mN) on a more elastic sample (SiO_2) is liable to superposing the non-linearity of the system compliance with a contribution due to the elastic deformation that becomes increasingly

negligible due to the larger overall penetration depths. This results in a systematic trend in the mechanical characterization results of the stiffer sample, i.e., W, as shown in Figure 6. This degenerates for the M2-FS8. In this case, the estimated frame compliance is 0 nm/μN, due to the mathematical constraints. This is counterbalanced by a very large standard error, which motivates why the ANOVA cannot highlight systematic relevance for the indentation calibration dataset obtained by bootstrap. Such a frame compliance estimation of 0 nm/μN is due to the constraint of the regression requiring a positive C_f, as described in Section 1.1.3. Apparently, the M2-FS8 would have resulted in a negative frame compliance, which is physically inconsistent; hence, it is fixed to the minimum physical value, i.e., 0 nm/μN.

Methods based on two CRMs, i.e., the ISO 14577-2 method M4 and the ODR single-step method, are less sensitive to the force range. In fact, all estimated parameters are statistically compatible, as shown in Figure 4. Methods based on two CRMs are generally highly accurate on FS (with an absolute relative accuracy smaller than 1%), and slightly worse on W, as shown in Figure 7. In particular, the ODR single-step method, due to its definition, provides significantly more accurate estimates also on W, with benefits in terms of the relative uncertainty, which is halved when resorting to the ODR rather than the M4, i.e., from 50% to 25%.

A slight overestimation of the frame compliance is obtained when a larger range of forces is considered for W (W7), i.e., when smaller forces are also considered for W (1mN and 2.5 mN). For the mechanical characterization of W, this overestimation leads to a trend (for M4) or a bias (for ODR) likely due to the superposition of the strong non-linearity of the C_f, which cannot be characterized by the considered methods, and due to the incipient indentation size effect of W.

In summary, the best calibration results suggest limiting the applied force range to larger forces on W, while increasing the number of force levels on FS is, in general, beneficial in terms of both relative accuracy and relative uncertainty.

5. Conclusions

This work highlighted the criticalities of the current calibration framework for area shape function and frame compliance in nanoindentation based on indirect calibration methods.

The work showed that calibration methods based on the use of a single sample are less accurate and more uncertain than methods that require the use of two certified reference materials. In particular, methods based on the use of a single sample provide a relative accuracy that is worse by one order of magnitude and a relative uncertainty that is at least double. Furthermore, this work highlighted a strong dependency of methods based on the use of one sample on the considered force range. Lastly, the standard version of such approaches is autocalibration and although practical, it yields poor performance in terms of relative accuracy and uncertainty.

Summarizing the results from the work, a practical suggestion for the calibration of the area shape function and frame compliance can be outlined within an uncertainty evaluation framework as follows:

- Calibration methods based on two certified reference materials, e.g., ISO 14577-2 method 4, optimize the accuracy and uncertainty of characterization.
- Multiple calibration indentation datasets are needed to avoid the severe underestimation of calibration uncertainty.
- A cost-effective approach to cater for the effect of the calibration indentation dataset can be obtained by the bootstrap simulation of such datasets.

- Indentation on tungsten certified reference material shall be greater than 5 mN to avoid characterization bias.
- The single-step method, based on orthogonal distance regression, further improves the accuracy and uncertainty of the ISO 14577-2 method 4.

Future work will compare the performance of calibration methods on other materials with industrial relevance, such as Ge, aluminum alloys, and titanium alloys, provided that their mechanical characteristics have been calibrated using an independent calibration approach, e.g., the pulse–echo method.

Author Contributions: Conceptualization, G.M.; methodology, G.M., G.G. and M.G.; software, L.G. and G.M.; validation, L.G. and G.G.; formal analysis, G.M.; investigation, L.G.; resources, M.G.; data curation, L.G.; writing—original draft preparation, G.M.; writing—review and editing, L.G., G.G. and M.G.; visualization, L.G.; supervision, M.G. All authors have read and agreed to the published version of the manuscript.

Funding: This research received no external funding.

Informed Consent Statement: Not applicable.

Data Availability Statement: The data used in this study are openly available on Zenodo at 10.5281/zenodo.17054480. The code for generating bootstrap samples is openly available on Zenodo at 10.5281/zenodo.17054597.

Conflicts of Interest: The authors declare no conflicts of interest.

Abbreviations

The following abbreviations are used in this manuscript:

CRM	Certified Reference Material
FS	Fused Silica (SiO2)
IIT	Instrumented Indentation Test
ISO	International Organization for Standardization

Appendix A

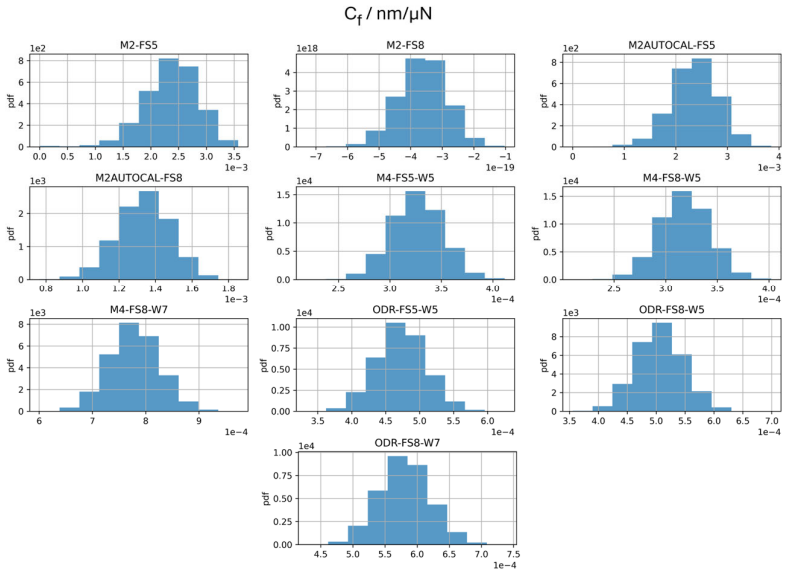


Figure A1. Empirical probability density function (pdf) of the 10,000 calibrated parameters for the 10 calibration methods for the frame compliance (C_f).

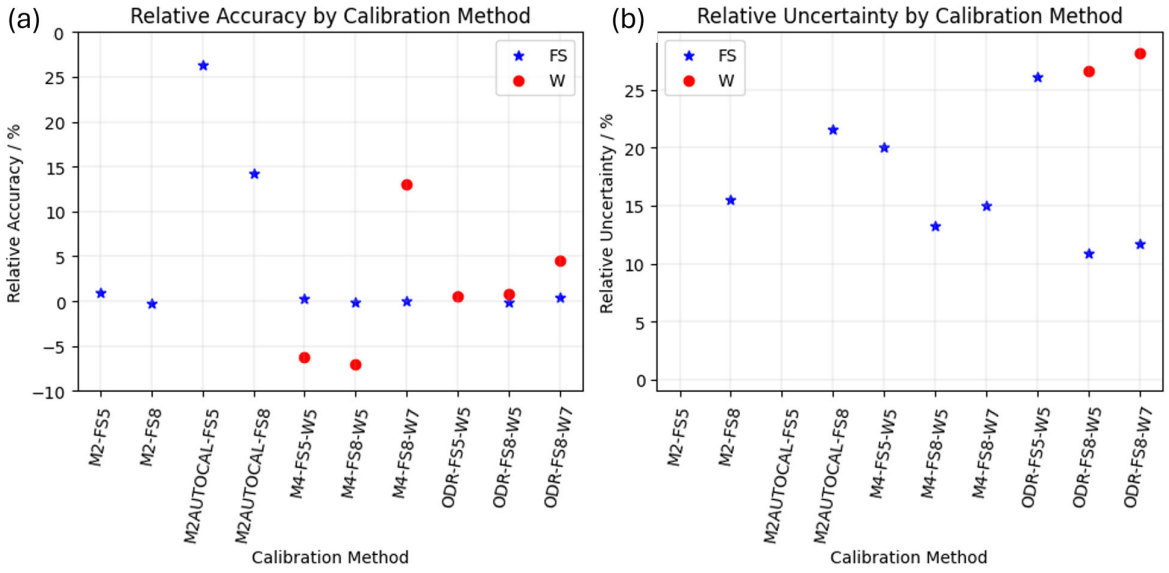


Figure A2. (**a**) Relative accuracy and (**b**) relative uncertainty for the E_{IT} of SiO_2 (FS blue star) and W (red circle). Not all values are represented to improve visualization (extreme values are excluded).

References

1. Oliver, W.C.; Pharr, G.M. An Improved Technique for Determining Hardness and Elastic Modulus Using Load and Displacement Sensing Indentation Experiments. *J. Mater. Res.* **1992**, *7*, 1564–1583. [CrossRef]
2. Oliver, W.C.; Pharr, G.M. Measurement of Hardness and Elastic Modulus by Instrumented Indentation: Advances in Understanding and Refinements to Methodology. *J. Mater. Res.* **2004**, *19*, 3–20. [CrossRef]
3. Lucca, D.A.; Herrmann, K.; Klopfstein, M.J. Nanoindentation: Measuring Methods and Applications. *CIRP Ann. Manuf. Technol.* **2010**, *59*, 803–819. [CrossRef]
4. Schulze, V.; Aurich, J.; Jawahir, I.S.; Karpuschewski, B.; Yan, J. Surface Conditioning in Cutting and Abrasive Processes. *CIRP Ann.* **2024**, *73*, 667–693. [CrossRef]
5. *ISO 14577-1:2015*; Metallic Materials-Instrumented Indentation Test for Hardness and Materials Parameters—Part 1: Test Method. International Organization for Standardization: Geneva, Switzerland, 2015.
6. Mughal, M.; Amanieu, H.-Y.; Moscatelli, R.; Sebastiani, M. A Comparison of Microscale Techniques for Determining Fracture Toughness of $LiMn_2O_4$ Particles. *Materials* **2017**, *10*, 403. [CrossRef]
7. Mieczkowski, G.; Szpica, D.; Borawski, A. Comprehensive Analysis of Elastic–Plastic Behavior in Hybrid Metal Matrix Composites with Varied Reinforcement Geometry. *Materials* **2025**, *18*, 2763. [CrossRef]
8. Slater, C.; Bandi, B.; Dastur, P.; Davis, C. Multiphase Identification Through Automatic Classification from Large-Scale Nanoindentation Mapping Compared to an EBSD-Machine Learning Approach. *Metals* **2025**, *15*, 636. [CrossRef]
9. Li, Z.; Klapetek, P.; Brand, U.; Refino, A.D.; Xu, J.; Peiner, E. Nanomechanical Characterisation of Vertical Nanowires Used for Energy Harvesting. *Meas. Sens.* **2025**, *38*, 101671. [CrossRef]
10. Lucca, D.A.; Klopfstein, M.J.; Ghisleni, R.; Cantwell, G. Investigation of Polished Single Crystal ZnO by Nanoindentation. *CIRP Ann.* **2002**, *51*, 483–486. [CrossRef]
11. Yan, D.; Cuevas, A.; Stuckelberger, J.; Wang, E.C.; Phang, S.P.; Kho, T.C.; Michel, J.I.; Macdonald, D.; Bullock, J. Silicon Solar Cells with Passivating Contacts: Classification and Performance. *Prog. Photovolt. Res. Appl.* **2023**, *31*, 310–326. [CrossRef]
12. Khataee, A.R.; Fathinia, M.; Aber, S.; Zarei, M. Optimization of Photocatalytic Treatment of Dye Solution on Supported TiO2 Nanoparticles by Central Composite Design: Intermediates Identification. *J. Hazard. Mater.* **2010**, *181*, 886–897. [CrossRef] [PubMed]
13. George, J.; Mannepalli, S.; Mangalampalli, K.S.R.N. Understanding Nanoscale Plasticity by Quantitative In Situ Conductive Nanoindentation. *Adv. Eng. Mater.* **2021**, *23*, 2001494. [CrossRef]
14. Lucca, D.A.; Zare, A.; Klopfstein, M.J.; Shao, L.; Xie, G.Q. Investigation of the Mechanical Behavior of Ion Irradiated Ni-Free Ti-Based Metallic Glass by Nanoindentation. *CIRP Ann.* **2014**, *63*, 533–536. [CrossRef]
15. Genta, G.; Maculotti, G. Thin Coatings Thickness Measurement by Augmented Nanoindentation Data Fusion. *CIRP Ann. Manuf. Technol.* **2024**, *73*, 409–412. [CrossRef]
16. Li, N.; Wang, C.; Li, C. Microstructures and High-Temperature Mechanical Properties of Inconel 718 Superalloy Fabricated via Laser Powder Bed Fusion. *Materials* **2024**, *17*, 3735. [CrossRef]

17. Rickhey, F.; Marimuthu, K.; Lee, H. Investigation on Indentation Cracking-Based Approaches for Residual Stress Evaluation. *Materials* **2017**, *10*, 404. [CrossRef]
18. Lee, Y.-H.; Kwon, D. Estimation of Biaxial Surface Stress by Instrumented Indentation with Sharp Indenters. *Acta Mater.* **2004**, *52*, 1555–1563. [CrossRef]
19. Sleem, K.; Grima, G.; Cabibbo, M. A Nanoindentation Approach to Investigating Dislocation Density in Additive-Manufactured SS316L-Graded Lattice Structures. *J. Manuf. Mater. Process.* **2025**, *9*, 59. [CrossRef]
20. Bertolini, R.; Bruschi, S.; Ghiotti, A.; Savio, E.; Ceseracciu, L.; Jawahir, I.S. Surface Integrity and Superelastic Response of Additively Manufactured Nitinol after Heat Treatment and Finish Machining. *CIRP Ann.* **2023**, *72*, 501–504. [CrossRef]
21. Lucca, D.A.; Klopfstein, M.J.; Ghisleni, R.; Gude, A.; Mehner, A.; Datchary, W. Investigation of Sol-Gel Derived ZrO_2 Thin Films by Nanoindentation. *CIRP Ann. Manuf. Technol.* **2004**, *53*, 475–478. [CrossRef]
22. Hayes, S.A.; Goruppa, A.A.; Jones, F.R. Dynamic Nanoindentation as a Tool for the Examination of Polymeric Materials. *J. Mater. Res.* **2004**, *19*, 3298–3306. [CrossRef]
23. Ovsik, M.; Manas, M.; Stanek, M.; Dockal, A.; Vanek, J.; Mizera, A.; Adamek, M.; Stoklasek, P. Polyamide Surface Layer Nano-Indentation and Thermal Properties Modified by Irradiation. *Materials* **2020**, *13*, 2915. [CrossRef]
24. Tosini, M.; Tänzer, T.; Villata, S.; Baruffaldi, D.; Monica, V.; Peracino, B.; Primo, L.; Frascella, F.; Pirri, F.; Audenino, A.; et al. A Methodological Approach for Interpreting and Comparing the Viscoelastic Behaviors of Soft Biological Tissues and Hydrogels at the Cell-Length Scale. *Appl. Sci.* **2024**, *14*, 1093. [CrossRef]
25. Xu, D.; Harvey, T.; Begiristain, E.; Domínguez, C.; Sánchez-Abella, L.; Browne, M.; Cook, R.B. Measuring the Elastic Modulus of Soft Biomaterials Using Nanoindentation. *J. Mech. Behav. Biomed. Mater.* **2022**, *133*, 105329. [CrossRef] [PubMed]
26. Qian, L.; Zhao, H. Nanoindentation of Soft Biological Materials. *Micromachines* **2018**, *9*, 654. [CrossRef] [PubMed]
27. Mostakhdemin, M.; Nand, A.; Ramezani, M. Articular and Artificial Cartilage, Characteristics, Properties and Testing Approaches—A Review. *Polymers* **2021**, *13*, 2000. [CrossRef]
28. Erazo, O.; Jakes, J.E.; Plaza, N.Z.; Vergara-Figueroa, J.; Valenzuela, P.; Gacitúa, W. Quasistatic and Dynamic Nanoindentation Measurements of *Pinus radiata* D. Don S2 and CCML Cell Wall Layers. *Forests* **2023**, *14*, 1900. [CrossRef]
29. Ezenwafor, T.; Anye, V.; Madukwe, J.; Amin, S.; Obayemi, J.; Odusanya, O.; Soboyejo, W. Nanoindentation Study of the Viscoelastic Properties of Human Triple Negative Breast Cancer Tissues: Implications for Mechanical Biomarkers. *Acta Biomater.* **2023**, *158*, 374–392. [CrossRef]
30. Yallapu, M.M.; Katti, K.S.; Katti, D.R.; Mishra, S.R.; Khan, S.; Jaggi, M.; Chauhan, S.C. The Roles of Cellular Nanomechanics in Cancer. *Med. Res. Rev.* **2015**, *35*, 198–223. [CrossRef]
31. *ISO 14577-2:2015*; Metallic Materials-Instrumented Indentation Test for Hardness and Materials Parameters—Part 2: Verification and Calibration of Testing Machines. International Organization for Standardization: Geneva, Switzerland, 2015.
32. Barbato, G.; Genta, G.; Cagliero, R.; Galetto, M.; Klopfstein, M.J.; Lucca, D.A.; Levi, R. Uncertainty Evaluation of Indentation Modulus in the Nano-Range: Contact Stiffness Contribution. *CIRP Ann. Manuf. Technol.* **2017**, *66*, 495–498. [CrossRef]
33. Barbato, G.; Brondino, G.; Galetto, M.; Vicario, G. "Zero-Point" in the Evaluation of Martens Hardness Uncertainty. In Proceedings of the 11th IMEKO TC5 Conference on Hardness Measurement 2002—Joint International Conference on Force, Mass, Torque, Hardness and Civil Engineering Metrology in the Age of Globalization, Celle, Germany, 24–26 September 2002; pp. 72–77.
34. Cagliero, R.; Barbato, G.; Maizza, G.; Genta, G. Measurement of Elastic Modulus by Instrumented Indentation in the Macro-Range: Uncertainty Evaluation. *Int. J. Mech. Sci.* **2015**, *101–102*, 161–169. [CrossRef]
35. Genta, G.; Maculotti, G.; Barbato, G.; Levi, R.; Galetto, M. Effect of Contact Stiffness and Machine Calibration in Nano-Indentation Testing. *Procedia CIRP* **2018**, *78*, 208–212. [CrossRef]
36. Maculotti, G.; Genta, G.; Lorusso, M.; Pavese, M.; Ugues, D.; Galetto, M. Instrumented Indentation Test: Contact Stiffness Evaluation in the Nano-Range. *Nanomanuf. Metrol.* **2018**, *2*, 16–25. [CrossRef]
37. Germak, A.; Herrmann, K.; Dai, G.; Li, Z. Development of Calibration Methods for Hardness Indenters. In *VDI Berichte*; Verlag: Düsseldorf, Germany, 2006; pp. 13–26.
38. Maculotti, G.; Kholkhujaev, J.; Genta, G.; Galetto, M. Direct Calibration of Indenter Tip Geometry by Optical Surface Topography Measuring Instruments. *J. Mater. Res.* **2023**, *38*, 3336–3348. [CrossRef]
39. Aldrich-Smith, G.; Jennett, N.J.; Hangen, U. Direct Measurement of Nanoindentation Area Function by Metrological AFM. *Int. J. Mater. Res.* **2005**, *96*, 1267–1271. [CrossRef]
40. Degenhardt, J.; Hu, X.; Zackaria, M.; Menelao, F.; Tutsch, R.; Dai, G. Accurate AFM Calibration of Indenter Geometry for Instrumented Indentation. *Nanomanuf. Metrol.* **2025**, *8*, 15. [CrossRef]
41. Vanlandingham, M.R.; Juliano, T.F.; Hagon, M.J. Measuring Tip Shape for Instrumented Indentation Using Atomic Force Microscopy. *Meas. Sci. Technol.* **2005**, *16*, 2173–2185. [CrossRef]
42. Barone, A.C.; Salerno, M.; Patra, N.; Gastaldi, D.; Bertarelli, E.; Carnelli, D.; Vena, P. Calibration Issues for Nanoindentation Experiments: Direct Atomic Force Microscopy Measurements and Indirect Methods. *Microsc. Res. Tech.* **2010**, *73*, 996–1004. [CrossRef]

43. Li, Z.; Brand, U. Towards Quantitative Characterisation of the Small Force Transducer Used in Nanoindentation Instruments. *Mod. Instrum.* **2013**, *02*, 61–67. [CrossRef]
44. Brand, U.; Chudoba, T.; Griepentrog, M.; Schwenk, D.; Bosch, G.; Scheerer, H.; Gärtner, E. Round Robin for Testing Instrumented Indenters with Silicon Reference Springs. *Int. J. Mater. Res.* **2015**, *106*, 1215–1223. [CrossRef]
45. Galetto, M.; Barbato, G.; Maculotti, G. System, Method and Device for Measuring the Frame Compliance of a Durometer. WO2024116066A1, 28 November 2023.
46. Doerner, M.F.; Nix, W.D. A Method for Interpreting the Data from Depth-Sensing Indentation Instruments. *J. Mater. Res.* **1986**, *1*, 601–609. [CrossRef]
47. Meneve, J.L.; Smith, J.F.; Jennett, N.M.; Saunders, S.R.J. Surface Mechanical Property Testing by Depth Sensing Indentation. *Appl. Surf. Sci.* **1996**, *100–101*, 64–68. [CrossRef]
48. Jennett, N.M.; McCartney, L.N.; Lawrence, K.; Hunt, R.; Maxwell, A.; Koskinen, J.; Meneve, J.; Wegener, W.; Gibson, N.; Bushby, A.J.; et al. Indicoat Final Report—Determination of Hardness and Modulus of Thin Films and Coatings by Nanoindentation. In *NPL Report MATC(A)*; National Physical Laboratory: Teddington, UK, 2001.
49. Herrmann, K.; Jennet, N.M.; Wegener, W.; Meneve, J.; Hasche, K.; Seeman, R. Progress in Determination of the Area Function of Indenters Used for Nanoindentation. *Thin Solid Film.* **2000**, *377–378*, 394–400. [CrossRef]
50. Galetto, M.; Genta, G.; Maculotti, G. Single-Step Calibration Method for Nano Indentation Testing Machines. *CIRP Ann.* **2020**, *69*, 429–432. [CrossRef]
51. Maculotti, G.; Genta, G.; Carbonatto, A.; Galetto, M. Uncertainty-Based Comparison of the Effect of the Area Shape Function on Material Characterisation in Nanoindentation Testing. In Proceedings of the 22nd International Conference and Exhibition of EUSPEN, Genève, Switzerland, 30 May–3 June 2022.
52. Boggs, P.T.; Byrd, R.H.; Schnabel, R.B. A Stable and Efficient Algorithm for Nonlinear Orthogonal Distance Regression. *SIAM J. Sci. Stat. Comput.* **1987**, *8*, 1052–1078. [CrossRef]
53. Maculotti, G.; Genta, G.; Galetto, M. Criticalities of Iterative Calibration Procedures for Indentation Testing Machines in the Nano-Range. In Proceedings of the 20th International Conference and Exhibition of EUSPEN, Genève, Switzerland, 8–12 June 2020; pp. 2–5.
54. Maculotti, G.; Genta, G.; Galetto, M. An Uncertainty-Based Quality Evaluation Tool for Nanoindentation Systems. *Measurement* **2024**, *225*, 113974. [CrossRef]
55. *JCGM100*; Evaluation of Measurement Data—Guide to the Expression of Uncertainty in Measurement (GUM). JCGM: Sèvres, France, 2008. [CrossRef]

Disclaimer/Publisher's Note: The statements, opinions and data contained in all publications are solely those of the individual author(s) and contributor(s) and not of MDPI and/or the editor(s). MDPI and/or the editor(s) disclaim responsibility for any injury to people or property resulting from any ideas, methods, instructions or products referred to in the content.